



## Novel graphene oxide functionalization by urea and thiourea, and their applications as anticorrosive agents for carbon steel alloy in acidic medium

Ali A. Naser<sup>1</sup>, Hadi Z Al-Sawaad<sup>2</sup>, Alaa S. Al-Mubarak<sup>3</sup>

<sup>1</sup>Ministry of Education, Mayssan's Directorate of Education

<sup>2,3</sup>University of Basrah, College of Science, Department of Chemistry

Received 30 Dec 2019,  
Revised 29 Jan 2020,  
Accepted 30 Jan 2020

### Keywords

- ✓ Graphene oxide,
- ✓ Corrosion inhibitors,
- ✓ Carbon Steel,
- ✓ Hydrochloric acid,
- ✓ Adsorption.

[hadiziara@yahoo.com](mailto:hadiziara@yahoo.com),  
Phone: +9647801131734  
[aabra0595@gmail.com](mailto:aabra0595@gmail.com),  
Phone: +9647710498865

### Abstract

Graphene oxide (GO) was synthesized by the modified Hummer's method and then functionalized by initially reacting with urea and subsequently with thiourea to produce GO-amine (GOA) and GOB, respectively. These compounds were characterized by Raman shift, X-ray diffraction, field-emission scanning electron microscopy, and energy-dispersive x-ray spectroscopy techniques. The three chemicals were evaluated as anticorrosion inhibitors for carbon steel alloy (C1025) against an acidic medium (0.1 M hydrochloric acid) at 298 K through the electrochemical method (Tafel plot method). Results revealed that the efficiencies of GO, GOA, and GOB were 77.4%, 91.7%, and 87%, respectively, at their optimal concentration of 100 ppm. The effects of temperature on the corrosion reaction were also examined. The efficiency was found to decrease with increased temperature to 298, 308, 318, and 328 K. Kinetic parameters including activation energy ( $E_a$ ), activation enthalpy ( $\Delta H^*$ ), Gibbs free energy of activation ( $\Delta G^*$ ) and activation entropy ( $\Delta S^*$ ) were evaluated. Kinetic and thermodynamic parameters were used to calculate  $E_a$  in the presence or absence of each inhibitor to determine the physical adsorption mode on the surface of carbon steel. Results showed that the adsorption modes obeyed the Langmuir method of adsorption according to their  $R^2$  value, which approached unity.

### 1. Introduction

Carbon steels have many applications as structural components and industrial pipes [1]. However, alloys and metals deteriorate through corrosion because of their reaction with their environment through chemical or electrochemical changes. Corrosion occurs in a cell system, which includes an anode, a cathode, an electrical circuit, and an electrolyte solution [2], and entails high maintenance costs because it can destroy and shorten the lifespan of metal equipment [3].

The corrosion of metals and alloys can be prevented or minimized through different techniques, such as using corrosion inhibitors, which are chemicals that reduce or prevent corrosion when they are added at a sufficient concentration. Corrosion inhibitors can be classified into inorganic and organic types based on their chemical structures. Organic inhibitors are widely used because they have one or more heteroatoms, such as O, N, S, and P. Thus, these molecules have a high basicity because of their electron density caused by the presence of these heteroatoms.

Different corrosion inhibitors have been used against the corrosion of carbon steel in acid media. The performance of an organic inhibitor is related to its chemical structure and physicochemical properties, such as electron density, functional groups, and electronic structure [4-7].

The adsorption of an inhibitor at a metal/solution interface is due to the formation of covalent bonding or electrostatic interactions between the metal surface of carbon steel and an inhibitor [8]. Graphene

oxide (GO) is an excellent material composed of single or multiple flat layers of carbon atoms packed into a 2D honeycomb lattice with  $sp^2$ -bonded carbon. GO has been widely explored for its physicochemical properties and possible applications in many fields [9, 10].

GO is a layer of graphene that is heavily decorated with oxygen functionalities, such as hydroxyl (OH), carbonyl (C=O), and alkoxy (C–O–C) groups. GO has been extensively investigated because of its low cost, easy access, and its widespread ability to convert into graphene. The scalability of GO is also a desired feature that has been considerably researched because of its large surface area, high intrinsic mobility, high Young's modulus, high thermal conductivity, and high optical transmittance. The functionalization of GO (FGO), where GO is dispersed in an organic solvent, enhances its physicochemical properties and improves its thermal, mechanical, and electric properties [11-16].

Our study aimed to enhance the ability of GO as a corrosion inhibitor for carbon steel alloy by grafting it with polar functional groups. A microwave method was used to initially functionalize GO with urea and subsequently with thiourea. GO and its derivatives were used as corrosion inhibitors for carbon steel alloy against 0.1 M HCl. The corrosion of carbon steel alloy in a certain acidic medium was evaluated using the Tafel method.

## 2. Material and Methods

### 2.1. Chemicals

In the present work, chemicals were purchased from different sources as follows: graphite powder (99%), sodium nitrate (99.9%), and hydrogen peroxide (30%; Fluka); sulphuric acid (99.9%; Sigma Aldrich); hydrochloric acid (37%), potassium permanganate (99%), and ethanol (99%; BDH); urea (99%), thiourea (99%), and N,N-dimethyl formamide (DMF; 99%; Merck).

### 2.2. Synthesis of graphene oxide (GO)

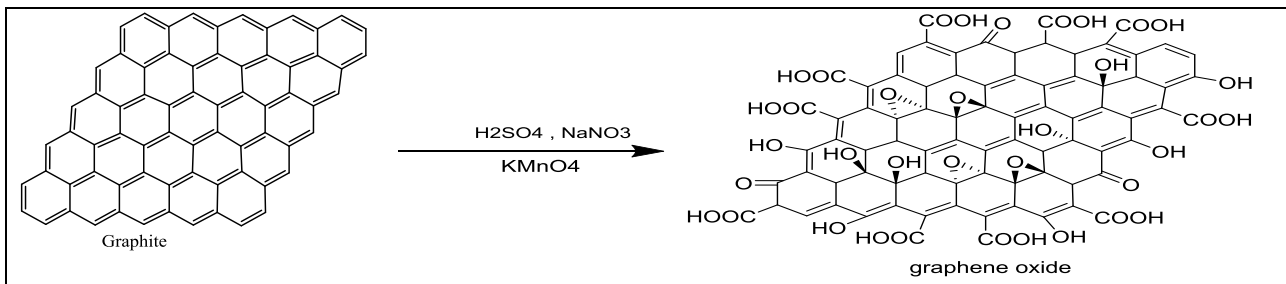
GO was prepared using the modified Hummer's method. Approximately 1 g of graphite powder, 23 mL of  $H_2SO_4$  and 0.5 g of sodium nitrate were mixed in a flask and stirred in an ice bath for 30 min. Approximately 3 g of  $KMnO_4$  was added gradually into the mixture for 3 h. A certain amount of hydrogen peroxide was added to the mixture to stop the reaction. The suspension was dried, exfoliated through sonication and repeatedly washed with 5% HCl and deionized  $H_2O$ . Afterwards, the product was dried in a furnace at 343–353 K for 4 h to obtain the solid GO [17-19].

### 2.3. Synthesis of GO-amine (GOA) and GOB

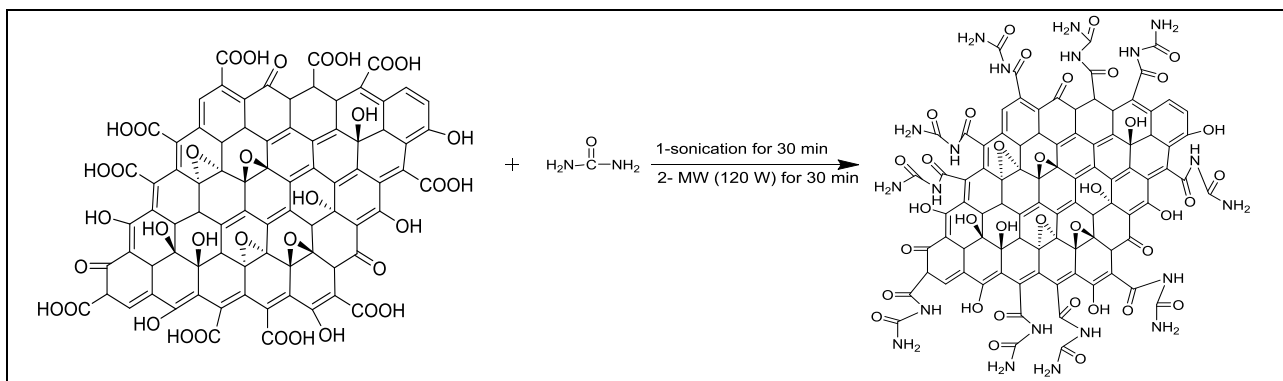
In a 100 mL beaker, 0.5 g of GO was dispersed in 50 mL of DMF through ultra-sonication for 30 min. Afterwards, 0.6 g of 10 mM urea was added to the mixture and dispersed by ultra-sonication for 30 min. The resulting suspension was heated in a microwave for 30 min at 20% power (140 W). The obtained suspension was repeatedly washed with 300 mL of anhydrous ethanol at different times in 1 day to remove any residual amount. The resulting suspension was then repeatedly washed with distilled water and ethanol to ensure the purity of the product. The final product GOA was dried at 70 °C for 6 h as black powder. Similarly, GO was grafted with 0.76 g of 10 mM thiourea to synthesize GOB [20]. The chemical reactions of GO, GOA, and GOB synthesis are shown in Schemes 1–3.

### 2.4. Characterization of GO and its derivatives

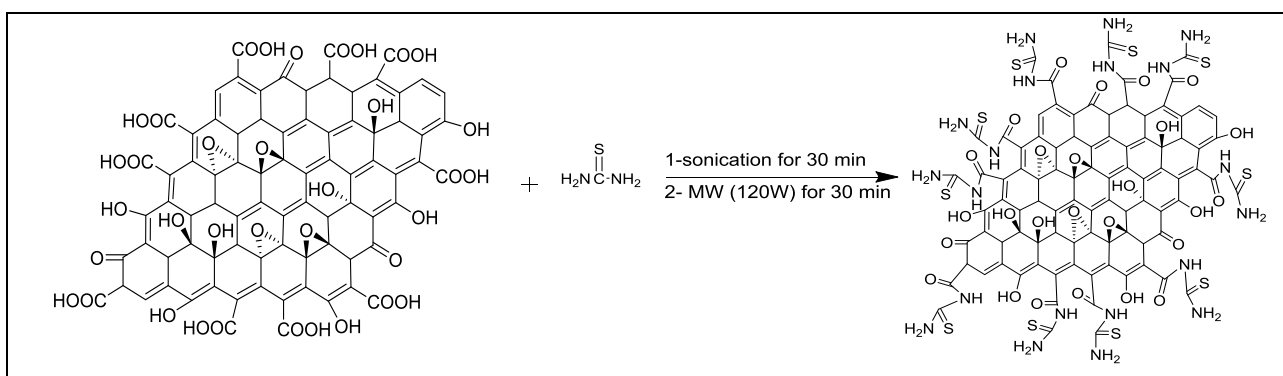
The synthesized compounds were characterized through Raman, field emission scanning electron microscopy (FESEM), energy-dispersive x-ray spectroscopy (EDX) and x-ray diffraction (XRD).



**Scheme1:** The general chemical reaction of synthesis GO compound.



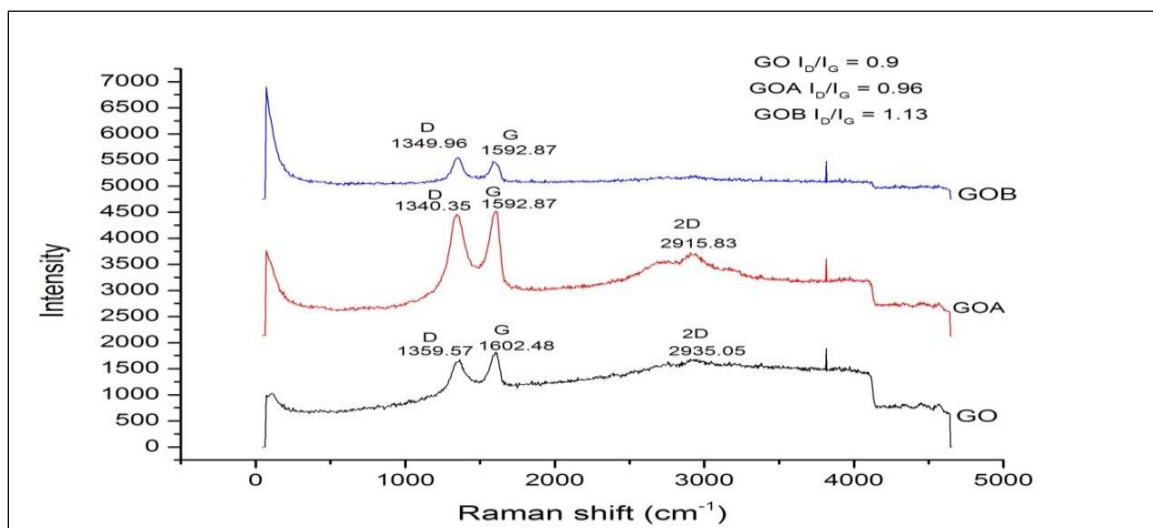
**Scheme2:** The general chemical reaction of synthesis GOA compound.



**Scheme3:** The general chemical reaction of synthesis GOB compound.

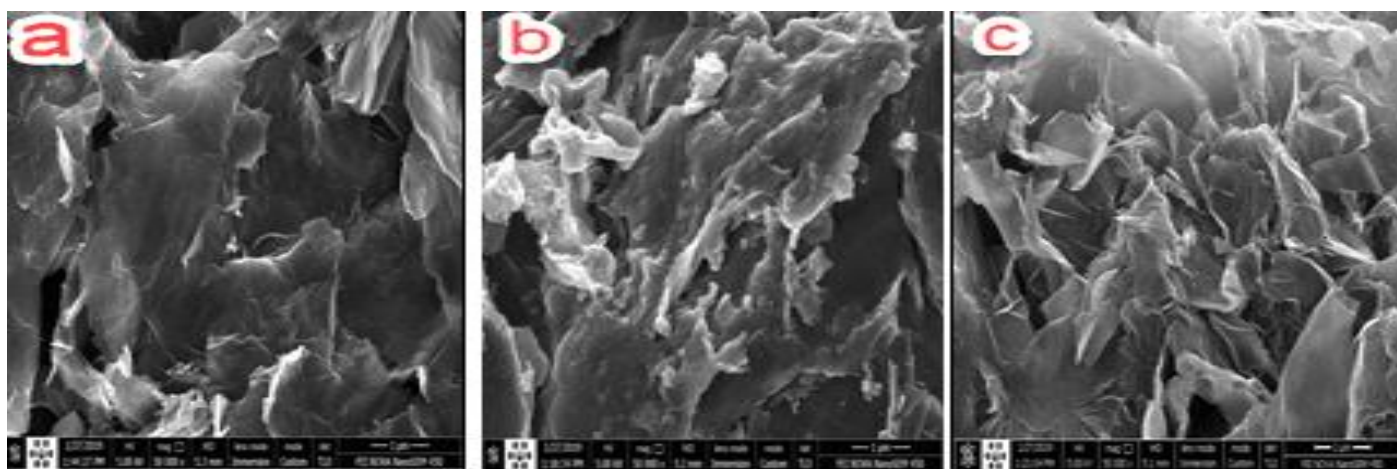
Raman spectroscopy is a good technique to characterize the structure and quality of carbon products and crystal structure, particularly to describe the defective, disordered, and ordered structures. Carbon products are represented as carbon-carbon double ( $\text{C}=\text{C}$ ) and conjugated bonds that lead to high Raman intensities. The electronic structures of compounds are highly sensitive, as shown by the Raman spectrum [12, 21-23]. Figure 1 reveals the Raman spectra of GO, GOA, and GOB. GO has two prominent bands, namely, D and G. The first band (D) at  $1359.57 \text{ cm}^{-1}$  is assigned to the disordered band (disordered structures of the  $\text{sp}^2$ ). The second band (G) at  $1602.48 \text{ cm}^{-1}$  is assigned to the first-order scattering of the in-phase vibration of the  $\text{E}_{2g}$  phonon and the vibration mode of carbon atoms ( $\text{sp}^2$ ) [12, 23, 24]. The Raman spectra of GOA and GOB derivatives depict that the two peaks of D and G bands in GOA exhibit a change in their behavior, in which the intensity of D in GOA is higher than that in GO and blue shifted compared with that in GO. The intensity of the G band of GOA is also higher than that in GO but has the same value as in GO. The intensities of D and G bands of GOB are higher than those of the same bands in GO but red shifted compared with those in GO. GOA and GOB have new 2D bands at approximately  $2915.83$  and  $2935.05 \text{ cm}^{-1}$ , respectively, compared with those of GO; thus, GO is grafted with urea in GOA and with thiourea in GOB because this band is not present in GO [25]. The Raman spectra of GO, GOA and GOB (Figure 1) depict that the intensities of  $\text{I}_D/\text{I}_G$  change because of

the electronic conjugation state of GO through modification. This increase in ID/IG is due to the increasing amount of urea and thiourea for GOA and GOB during preparation; that is, the intensities of ID/IG of GO, GOA, and GOB are 0.9, 0.96, and 1.13, respectively. This increase in ID/IG is also a result of the reduction of GO and amine grafting with GO during modification with urea and thiourea [26].



**Figure 1:** Raman spectra of GO, GOA, and GOB.

The morphological surface characteristics and properties of GO and its derivatives were studied through FESEM. As shown in Figure 2a, the FESEM image of GO has a smooth, thin, and flat sheet with kinked areas and numerous wrinkled edges. The surface of GO is light grey and composed of several layers [27, 28]. The FESEM images of GOA and GOB in (Figures 2b and 2c, respectively) reveal that GOA has multiple light grey layers and a dark grey part with sharp edges. Images also show wrinkled and stacked layers between them and one on top of the other. GOB also consists of many light grey layers and few dark grey layers. The outer surface is rough, and the parts and edges are folded. Small granules of light colored, corrugated, and wrinkled areas are also observed. The variability and difference in GOA and GOB compared with those of GO are good indications of the separate FGO by urea and thiourea, respectively. The average particle sizes were determined using the Image-J program. The average particle sizes of the compounds are listed in (Table 1), as revealed through FESEM, correspond to the results at scales of 500 and 400 nm in some compounds [27-29].

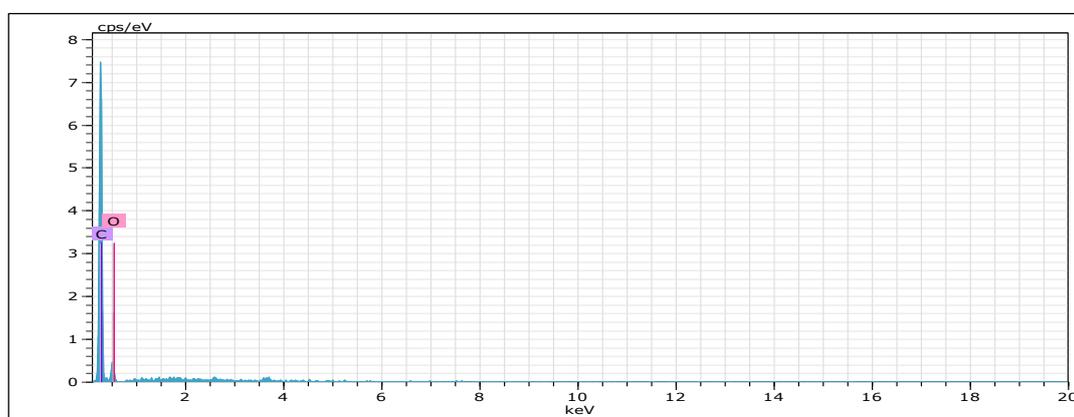


**Figure 2:** Field emission scanning electron microscopy (FESEM) images of the prepared a: GO, b: GOA, and c: GOB.

**Table 1:** Average nanoparticle size of GO, GOA, and GOB.

No	Com	Particle size (nm)	Average
1	GO	52,40,52,27.5,48,41.8	43.55
2	GOA	29.18, 46.57,31.46	35.74
3	GOB	66,8,55.55	61.18

GO, GOA, and GOB were characterized through EDX analysis with SEM. EDX was employed to analyze the elemental composition and chemical characteristics of compounds [30]. As shown in the EDX spectrum of GO in Figure 3 and Table 2, the two peaks related to C and O atoms have 0.277 and 0.525 KeV of energy with 71.45 wt.% and 28.55 wt.% for GO, and 76.83 wt.%, and 23.17 wt.% for GOA, respectively. This result indicates successful GO synthesis and agrees with published studies on GO synthesis [31]. The EDX spectra and data of GOA and GOB indicate a new change, as shown in Figures 4 and 5 and Tables 3 and 4, respectively. A new peak at 0.392 KeV for N is found in GOA, whereas two new peaks at 0.392 and 2.307 KeV for N and S are observed in GOB, respectively. This finding confirms that GO is separately functionalized by urea and thiourea. The weight percentages of GOA and GOB are as follows: 65.79 wt.% (C), 29.63 wt.% (O), 4.58 wt.% (N), 72.55 wt.% (C), 13.71 wt.% (O), 9.22 wt.% (S), and 4.52 wt.% (N). The atomic percentages of GOA and GOB are as follows: 71.57 at% (C), 24.16 at% (O), 4.27 at% (N), 80.46 at% (C), 11.41 at% (O), 3.83 at% (S), and 4.30 at% (N). Thus, these results evidently show the appearance of N and S for successful GO functionalization with amine (urea and thiourea) [10, 32, 33]. EDX elemental mapping was performed to understand the distribution of N in GOA and N and S in GOB on GO. The elemental mapping indicates the uniform distribution of N in GOA and N and S in GOB on GO. The elemental mapping indicates the uniform distribution of N and S over the GO surface and shows homogeneous distribution of N and S over the measured area of GO in GOB [28, 34], as shown in Figures 6a, 6b, and 6c.

**Figure 3:** EDX spectra of GO.**Table 2:** EDX spectral analysis of GO.

Element	AN.	Series	KeV	[norm.wt. %]	[norm.at. %]
C	6	K-series	0.277	71.45	76.83
O	8	K-series	0.525	28.55	23.17
Sum:				100	100

**Table 3:** EDX spectral analysis of GOA.

Element	AN.	Series	KeV	[norm.wt. %]	[norm.at. %]
C	6	K-series	0.277	65.79	71.57
O	8	K-series	0.525	29.63	24.16
N	7	K-series	0.392	4.52	4.27
Si	14	K-series	1.85	0	0
Sum:				100	100

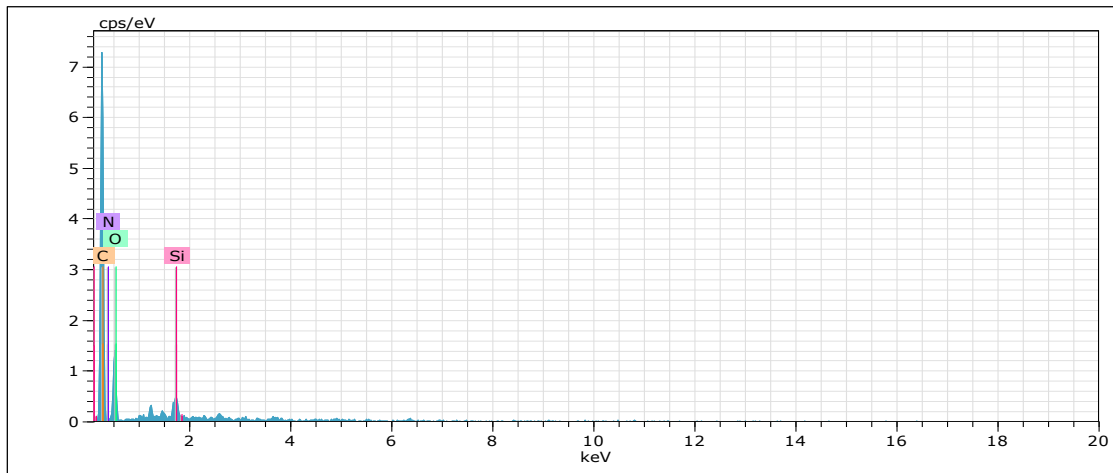


Figure 4: EDX spectra of GOA.

Table 4: EDX spectral analysis of GOB.

Element	AN.	Series	KeV	[norm.wt. %]	[norm.at. %]
C	6	K-series	0.277	72.55	80.46
O	8	K-series	0.525	13.71	11.41
S	16	K-series	2.307	9.22	3.83
N	7	K-series	0.392	4.52	4.30
Sum:				100	100

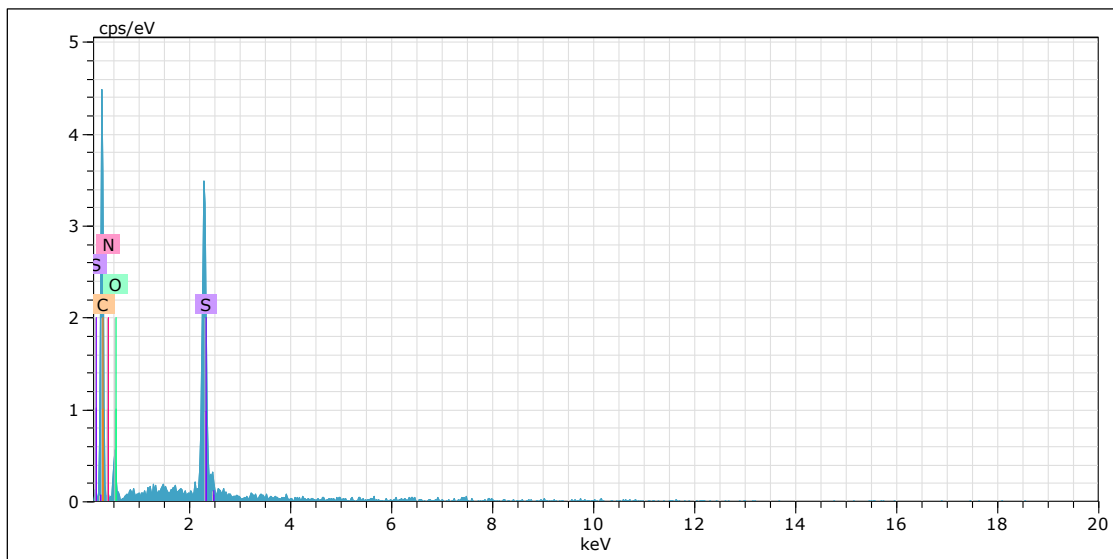


Figure 5: EDX spectra of GOB.

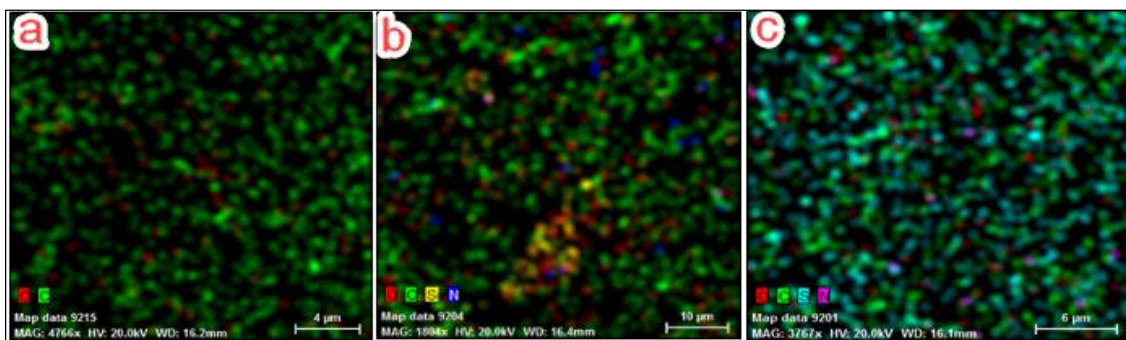
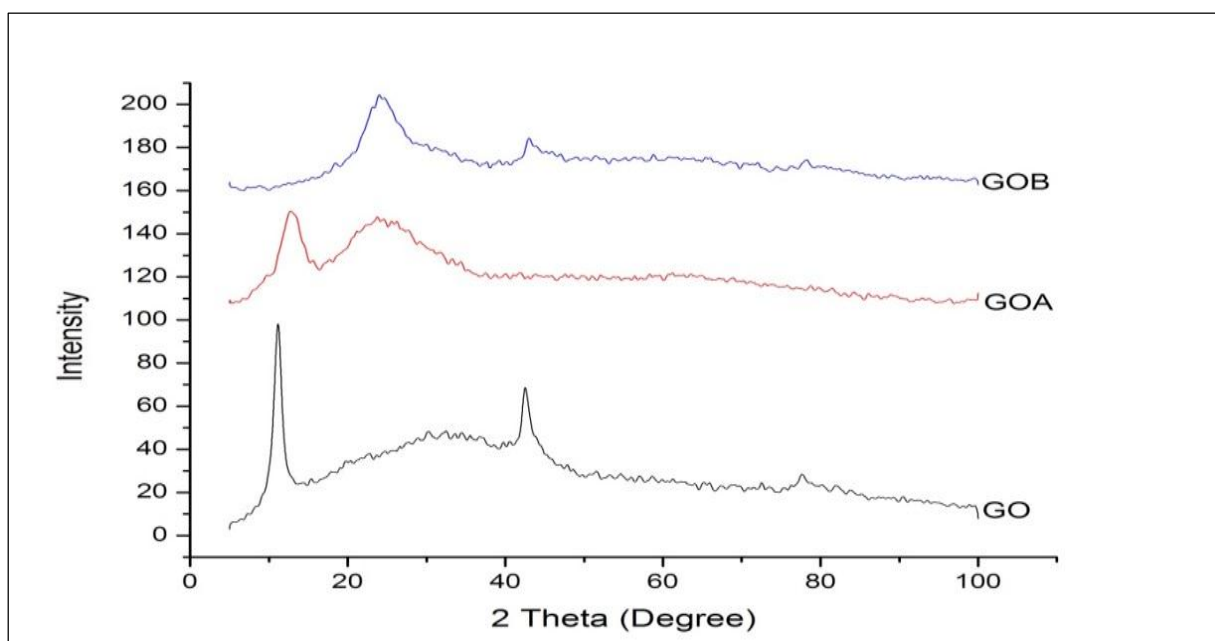


Figure 6: EDX elemental distribution mapping of the prepared a: GO, b: GOA, and c: GOB.

XRD was also conducted to identify GO and its derivatives. As shown in Figure 7, the spectra of GO, GOA, and GOB provide good information that can help determine the change in the GO structure compared with those of GOA and GOB. GO has a characteristic sharp peak at  $2\theta = 11.15^\circ$  corresponding to  $d$ -spacing =  $8.0 \text{ \AA}$ . GO is produced from the oxidation of graphite powder. Graphite has a reflection 002 peak at  $26.6^\circ$  corresponding to  $d$ -spacing =  $3.3 \text{ \AA}$ . In GO, the peak of graphite disappears, and a new reflection 002 peak appears at  $11.15^\circ$ . The interlayer spacing is increased to  $8 \text{ \AA}$  because of the presence of oxygen-rich groups containing functional groups on both sides of GO. This finding confirms the successful oxidation of graphite into GO [16, 25, 26, 35, 36]. The comparison of the XRD of GOA and GOB spectra with that of GO spectra reveals that  $2\theta$  of GO increases from  $11.15^\circ$  to  $12.85^\circ$  (GOA) after GO is functionalized by urea. This change indicates that the interlayer spacing decreases to  $6.9$  (GOA) [37]. By contrast,  $2\theta$  of GOB decreases to  $9.21^\circ$  compared with that of GO. When GOB is functionalized by thiourea, the interlayer spacing increases to  $9.6$  (GOB). The decrease and increase in GOA and GOB in the interlayer spacing compared with those of GO imply that amino groups successfully attach onto the GO surface [26, 32].



**Figure 7:** XRD spectra of GO, GOA, and GOB.

The new peaks at  $25.10$  and  $24.43$  (Figure 7) correspond to GOA and GOB, respectively, leading to the formation of a disordered stacking structure in GO functionalized with urea and thiourea. The crystallite size of GO, GOA, and GOB can be calculated using the XRD data and the Scherrer equation as follows [38]:

$$D = \frac{K\lambda}{\beta \cos\theta} \dots\dots\dots 1$$

where  $D$  is the crystallite size (nm),  $\lambda$  is the x-ray wavelength ( $0.15406 \text{ nm}$  for  $\text{Cu K}\alpha$ ),  $K$  is the Scherrer constant ( $0.9$ ) that depends on the shape of a crystal,  $\beta$  is the full width at half maximum of intensity, and  $\theta$  is the Bragg angle. Table 5 depicts that the crystallite sizes of GO and its functionalized compounds are  $7.28$ ,  $2.77$ , and  $0.48$  of GO, GOA, and GOB, respectively. The crystallite size of GO is higher than those of GOA and GOB because the GO surface is separately grafted with urea and thiourea.

**Table 5:** Structural parameters of the prepared compounds as derived from the XRD pattern.

No	Samples	2Theta degree	Distance(d002) (Å)	FWHM degree	CrystalliteSize (nm)
1	GO	11.15°	8	1.097	7.28
2	GOA	12.85°	6.9	2.891	2.77
3	GOB	9.21°	9.6	16.728	0.48

### 3. Corrosion study

#### 3.1. Experimental

##### 3.1.1. Composition of carbon steel alloy

A C1025 type of carbon steel alloy was used (Table 6).

**Table 6:** Composition of carbon steel (C1025).

Alloy	Composition % w/w							
	Carbon steel (C1025)	C	S	P	Mn	Si	other	Fe
		0.27	0.002	0.003	0.69	0.2	0.3499	Balance

#### 3.2. Preparation of working electrode

The carbon steel alloy (C1025) was cut into strips with length, width, and thickness of 2, 2.55, and 0.35 cm, respectively. The total strip area immersed in a corrosive medium was 12.4925 cm<sup>2</sup>. The alloy was ground and polished using silicon carbide paper with different smoothness grades (80, 120, 200, 400, and 600 grades). Thereafter, the strip was degreased with acetone, washed with distilled water and ethanol, dried, and placed in desiccators containing silica gel to protect the specimens against moisture through an interval between polarization measurements and alloy polishing.

#### 3.3. Electrochemical cells, potentiodynamic method (Tafel plot), and solution preparation

In this study, the electrochemical cell in the corrosion test consisted of a 100 mL vessel connected to three electrodes: platinum electrode, carbon steel specimen, and saturated calomel electrode as counter, working, and reference electrodes, respectively. GO, GOA, and GOB were used separately to prepare several concentrations (10, 30, 50, 70, and 100 ppm) at 298 K to evaluate their activity as corrosion inhibitors. The effect of temperature on the corrosion reaction in the presence and absence of optimal GOA and GOB concentrations was studied at 298, 308, 318, and 328K in 0.1 M HCl as a corrosive agent. Potentiodynamic and polarization measurement is a commonly used technique to measure corrosion resistance and various functions and determine the current density versus the electric potential through a setup of open circuit potential (OCP) for 20 min. The polarization curve can then be acquired by scanning the potential range between -2.5 mV and +2.5 mV (vs. OCP) by using a computer for potentiostat/galvanostat at a scanning rate of 10 mV S<sup>-1</sup>.

### 3. Results and discussion

As shown in Table 7 and Figure 8, the corrosion current density and corrosion rate (CR) of the carbon steel alloy is generally reduced in the presence of the inhibitor regardless of type (GO, GOA, or GOB) because the certain inhibitor tends to form a protective film on the carbon steel alloy. Consequently, the corrosion reaction is reduced by removing water molecules and hydrochloric acid solute from the alloy surface. Thus, the charge-transfer resistance is enhanced by the presence of the certain inhibitor. E<sub>corr</sub> (Table 7) of the corrosion cell in the presence of certain inhibitors is almost not lesser or greater than +9 mv compared with that of the blank (absence of inhibitor). This result indicates that the behavior of each

inhibitor is mixed [39]. Furthermore, the Tafel constant values, that is, the anodic and cathodic Tafel constants, increase in the case of GO, GOA, and GOB compared with those in the blank. These data suggest that the anodic dissolution of the metal and the evolution of hydrogen at the cathode are controlled by the presence of each inhibitor. This finding suggests that the inhibitors initially become adsorbed on the metal surface and subsequently impede the passage of metal ions from the oxide-free metal surface to the solution by blocking the reaction sites of the metal surface. Consequently, the anodic reaction mechanism is affected. This finding also demonstrates that our inhibitors are of mixed type [40, 41].

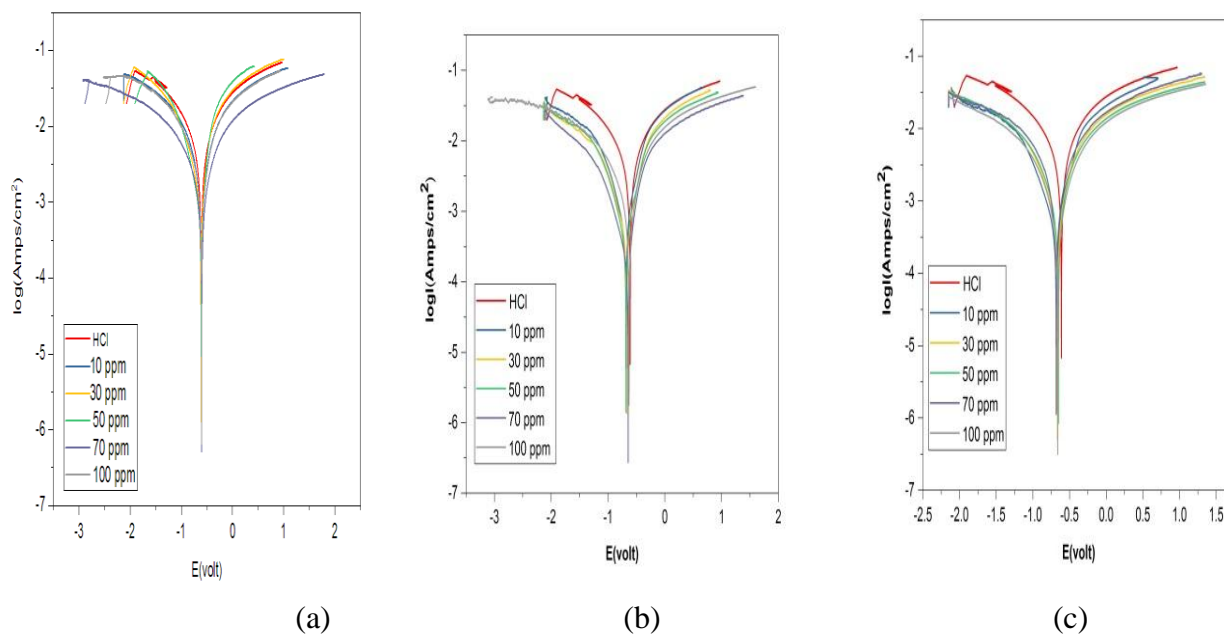


**Figure 8:** Tafel Plot in the absence and presence of inhibitors: a: GO, b: GOA, and c: GOB at 298 K.

**Table 7:** Corrosion parameters in the absence and presence of GO, GOA, and GOB at 298 K.

comp	Conc (ppm)	$E_{corr}$ (mV)	$I_{corr}$ ( $\mu A.Cm^{-2}$ )	CR (mpy)	$\beta_a$ mV	$\beta_c$ mV	$R_p$ ( $\Omega.cm^2$ )	% IE	$\theta$
HCl	Blank	- 611	1092	505.54	214.94	- 240.19	16.488	-	-
GO	10	- 605	412.1	190.82	335.45	- 367.41	43.682	62.3	0.623
	30	- 617	391.5	181.28	214.02	- 394.33	45.982	64.2	0.642
	50	- 605	394.2	182.52	366.64	- 411.11	45.668	63.9	0.639
	70	- 609	309.7	143.41	161.77	- 377.31	58.124	71.7	0.717
	100	- 603	246.7	114.24	443.65	- 458.22	72.963	77.4	0.774
GOA	10	- 685	227.3	105.25	379.61	- 1337.5	79.196	79.2	0.792
	30	- 672	188.3	87.171	488.97	- 1363.8	95.621	82.8	0.828
	50	- 683	155.1	71.794	358.65	- 962.12	116.1	85.8	0.858
	70	- 630	221.2	102.42	345.76	- 381.52	81.387	79.8	0.798
	100	- 647	90.42	41.87	219.9	- 872.54	199.08	91.7	0.917
GOB	10	- 680	172.9	80.051	307.09	- 952.98	104.13	84.2	0.842
	30	- 667	181	83.818	272.97	- 321.24	99.446	83.4	0.834
	50	- 652	195.8	90.628	292.13	- 265.54	91.974	82.1	0.821
	70	- 682	237.2	109.83	290.07	- 417.41	75.892	78.3	0.783
	100	- 661	141.8	65.659	262.32	- 317.41	126.95	87	0.870

The inhibition efficiency increases from 62.3% to 77.4% in GO and from 79.2% to 91.7% in GOA as their concentrations increase from 10 ppm to 100 ppm (optimal concentration), respectively, (Table 7) because the number of the adsorbed molecule, as a protective film, increases as the concentration increases. The corrosion reaction is also reduced. When the concentrations of GO and GOA reach 50 and 70 ppm, respectively, their efficiencies decrease to 63.9% and 79.8%, respectively, because the protective film starts to breakdown because of the loss in ability to thicken [42]. Although the efficiency of GOB decreases from 84.2% at 10 ppm to 78.3% at 70 ppm because of the same reasons, the efficiency enhances by 87.0% (Table 7) as its concentration reaches 100 ppm. This finding may be attributed to the increase in the number of GOB molecules in the corrosive medium that provides a simple blocking site for the reaction. The polarization resistance ( $R_p$ ) significantly increases when the inhibitor is used. By contrast, CR decreases in the presence of the inhibitor [43].

### 3.5. Effect of temperature on corrosion reaction

The effect of temperature on the corrosion reaction of the carbon steel alloy was studied in the presence of the optimal concentrations of GO, GOA, and GOB and compared with that in the blank. Table 8 and Figure 9 represent the Tafel data and plots produced from the electrochemical measurement of the carbon steel alloy surface, respectively. Generally, Table 8 shows that the efficiencies of GO, GOA, and GOB are reduced as temperature increased from 298 K to 328 K. The corrosion current density and CR increase, and the  $R_p$  of the alloy surface decreases. This result is expected because this effect increases the kinetic energy of the inhibitory particles and reduces both the efficiency of adsorption and surface coverage area covered by the inhibitor molecules as temperature increases [43, 44]. In addition, these inhibitors are physically adsorbed on the carbon steel alloy [45], that is, the protective film of the certain inhibitor tends to form electrostatic attraction forces with the alloy rather than a covalent bond. Conversely, the first force is weaker than the second one. Figure 10 shows the relation between CR and temperature.

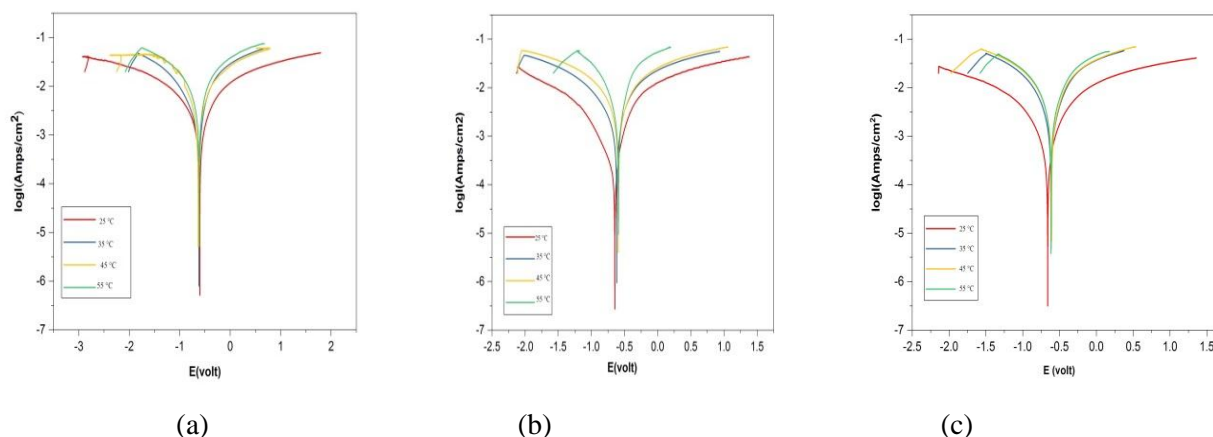


Figure 9: Tafel Plot in the presence of optimal concentrations of GO, GOA, and GOB at different temperatures.

### 3.6. Kinetic study of the corrosion reaction of carbon steel alloy

In the present work, kinetic parameters, including activation energy ( $E_a$ ), activation enthalpy ( $\Delta H^*$ ), activation entropy ( $\Delta S^*$ ), and Gibbs free energy of activation ( $\Delta G^*$ ), were calculated for the corrosion reaction of carbon steel alloy in the presence of the inhibitors, and their values were independently compared with those in the absence of the inhibitors in accordance with the electrochemical data shown in Table 8 at 298, 303, 308, and 313 K.

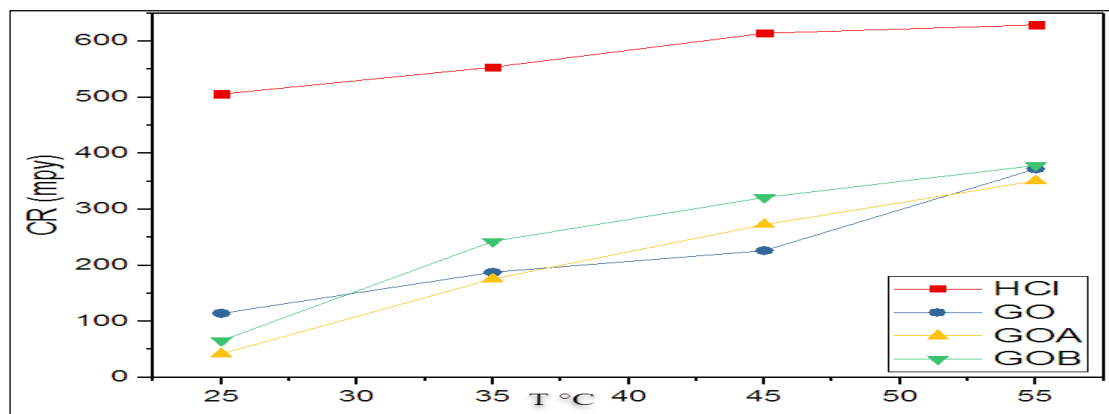


Figure 10: Effect of temperature on the corrosion rate in the absence and presence of GO, GOA, and GOB.

Table 8: Effect of temperature on the corrosion rate in the absence and presence of GO, GOA, and GOB.

Comp	Temp (°C)	E <sub>corr</sub> (mV)	I <sub>corr</sub> (μA.Cm <sup>-2</sup> )	CR (mpy)	β <sub>a</sub> (mV)	β <sub>c</sub> (mV)	R <sub>p</sub> (Ω.cm <sup>2</sup> )	% IE	θ
HCl	25	- 611	1092	505.54	214.94	- 240.19	16.488	-	-
	35	- 620	1196	553.53	249.49	- 248.25	15.059	-	-
	45	- 599	1327	614.18	231	- 259.9	13.571	-	-
	55	- 614	1359	629.03	242.06	- 366.58	13.251	-	-
GO	25	- 603	246.7	114.24	443.65	- 458.22	72.963	77.4	0.774
	35	- 619	405.1	187.58	236.52	- 437.9	44.436	66.1	0.661
	45	- 631	488.4	226.16	293.22	- 287.56	36.856	63.2	0.632
	55	- 614	803.4	372.03	313.81	- 423.78	22.405	40.9	0.409
GOA	25	- 647	904.2	41.87	219.9	- 872.54	199.08	91.7	0.917
	35	- 617	379.4	175.66	274.18	- 445.71	47.452	68.3	0.683
	45	- 595	588.6	272.53	395.39	- 434.27	30.585	55.6	0.556
	55	- 591	757.4	350.72	188.27	- 225.08	23.767	44.3	0.443
GOB	25	- 661	141.8	65.659	262.32	- 317.41	126.95	87	0.87
	35	- 614	524.2	242.72	247.01	- 261.59	34.341	56.2	0.562
	45	- 607	693.7	321.22	268.75	- 261.56	25.949	47.7	0.477
	55	- 616	816.8	378.2	318.65	- 325.47	22.04	39.9	0.399

These kinetic parameters were calculated for the presence of the optimal concentration of a certain inhibitor. E<sub>a</sub> was calculated on the basis of the Arrhenius relationship as in Equation 1:

$$\ln CR = \ln A - \frac{E_a}{RT} \dots \dots \dots 1$$

Where CR is the corrosion rate (mpy), E<sub>a</sub> is the activation energy of the corrosion reaction (kJ·mol<sup>-1</sup>), A is the Arrhenius pre-exponential constant, T is the absolute temperature (K) and R is the universal gas constant (8.3143 J·K<sup>-1</sup>·mol<sup>-1</sup>). E<sub>a</sub> can be calculated by plotting ln CR versus 1/T, where the slope is equal to (-E<sub>a</sub>/R). Thus, E<sub>a</sub> of the corrosion reaction of carbon steel alloy was calculated in the absence and presence of the optimal concentrations of GO, GOA and GOB. Results are acquired by plotting Equation 1 in Figure 11, and the data are summarized in Table 9. E<sub>a</sub> of corrosion increases when GO, GOA, or GOB inhibitor is added to the corrosive medium, which corresponds to a decrease in CR of the alloy in the presence of any of the inhibitors. E<sub>a</sub> in the presence of GOA or GOB is greater than that in the presence of GO. This finding is a good indication that GO functionalized by either urea (GOA) or thiourea (GOB) enhances the inhibitory ability of GO against the corrosive effect of HCl. The range of E<sub>a</sub> in the absence and presence of the inhibitor from 6.29 kJ·mol<sup>-1</sup> to 55.84 kJ·mol<sup>-1</sup> is lower than the

threshold of  $80 \text{ kJ}\cdot\text{mol}^{-1}$  required for chemisorption. This result indicates the physical adsorption of GO and GOA onto the surface [46-50].

Other kinetic parameters, such as  $\Delta H^*$ ,  $\Delta S^*$ , and  $\Delta G^*$ , for the corrosion reaction of carbon steel alloy were calculated using Equations 2 and 3:

$$\ln \frac{CR}{T} = \ln \frac{R}{Nh} + \left(\frac{\Delta S^*}{R}\right) - \left(\frac{\Delta H^*}{RT}\right), \dots \dots \dots 2$$

$$\Delta G^* = \Delta H^* - T\Delta S^*, \dots \dots \dots 3$$

Where  $N$  is Avogadro's number ( $6.022 \times 10^{23} \text{ mol}^{-1}$ ), and  $h$  is Plank's constant ( $6.62 \times 10^{-34} \text{ J}\cdot\text{s}$ ). Thus,  $\Delta H^*$  and  $\Delta S^*$  were calculated by plotting  $\ln CR/T$  versus  $1/T$ , as shown in Figure 9.  $\Delta G^*$  was calculated by using Equation 3 to obtain the slope and intercept equal to  $(-\Delta H^*/R)$  and  $(\ln R/Nh + \Delta S^*/R)$ , respectively.  $\Delta H^*$ ,  $\Delta G^*$ , and  $\Delta S^*$  are summarized in Table 9.

Table 9 shows that the corrosion reaction on the surface of carbon steel alloy is endothermic even in the presence or absence of any of the synthesized inhibitors. However, the endothermic behaviour increases in the presence of each of the inhibitors. This condition indicates that the corrosion reaction increases as temperature increases and implies that the dissolution of carbon steel is slow in the presence of inhibitors. Each inhibitor is physically adsorbed on the alloy surface [45]. These calculated data revealed that  $\Delta S^*$  for dissolution reaction of carbon steel in 0.1 M HCl in the presence inhibitors is higher than that in the absence of inhibitors. Large and negative values of  $\Delta S^*$  show that the activated complex in the rate-determining step represents an association than a dissociation step. This finding means that a decrease in disorder takes place to change reactants to the activated complex. This behavior may be explained as a result of the replacement process of water molecules through adsorption of GO derivatives on steel [51,52].  $\Delta G^*$  (Table 9) reveals that corrosion reaction becomes more nonspontaneous in the presence of the inhibitor.

Tables 8 and 9 show the corrosion current density and CRs of GO, GOA, and GOB. These values decrease in the presence of the inhibitor, whereas the charge-transfer resistance of the alloy increases. The best inhibitor decreases in the order  $\text{GOA} > \text{GOB} > \text{GO}$  because of the inhibition efficiency. The  $E_a$  of the corrosion reaction increases in the same order as above compared with that in the absence of an inhibitor. This result indicates that GO is preferably functionalized with urea rather than with thiourea.

**Table 9:** Kinetic parameters in the absence and presence of optimum inhibitor concentrations.

Comp	Optimum conc (ppm)	Ea (KJ.mol <sup>-1</sup> )	ΔH* (KJ.mol <sup>-1</sup> )	ΔS* J.k-1.mol <sup>-1</sup> )	ΔG* ( KJ.mol <sup>-1</sup> )			
					298K	308K	318K	328K
HCl	0	6.29	3.62	- 180.95	57.55	59.36	61.17	62.98
GO	70	30.30	27.8	- 112.18	61.23	62.35	63.47	64.6
GOA	70	55.84	53.38	- 32.22	62.99	63.30	63.63	63.95
GOB	100	45.51	42.97	- 63.43	61.88	62.51	63.15	63.78

### 3.7. Adsorption ability of the inhibitors on the alloy

The surface coverage area on the alloy by the inhibitor  $\theta$  was calculated at optimal concentrations of GO and its derivatives in the last range of temperatures. The data are listed in Table 7. The degree of the surface coverage is reduced with increased temperature from 298 K to 328 K at optimal concentrations. In the present study,  $\theta$  is calculated using Equation (4).

$$\theta = \frac{CR_{unhib} - CR_{inhib}}{CR_{unhib}} \dots\dots\dots 4$$

Where  $CR_{unhib}$  and  $CR_{inhib}$  are CR in the absence and presence of the inhibitors, respectively.

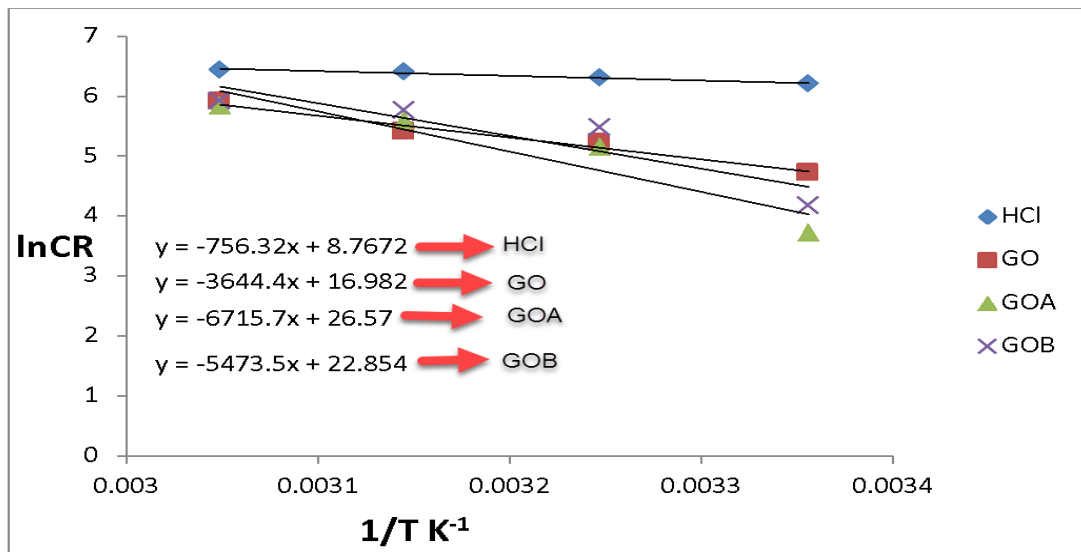


Figure 11: Calculation of  $E_a$  in the absence and presence of GO, GOA, and GOB.

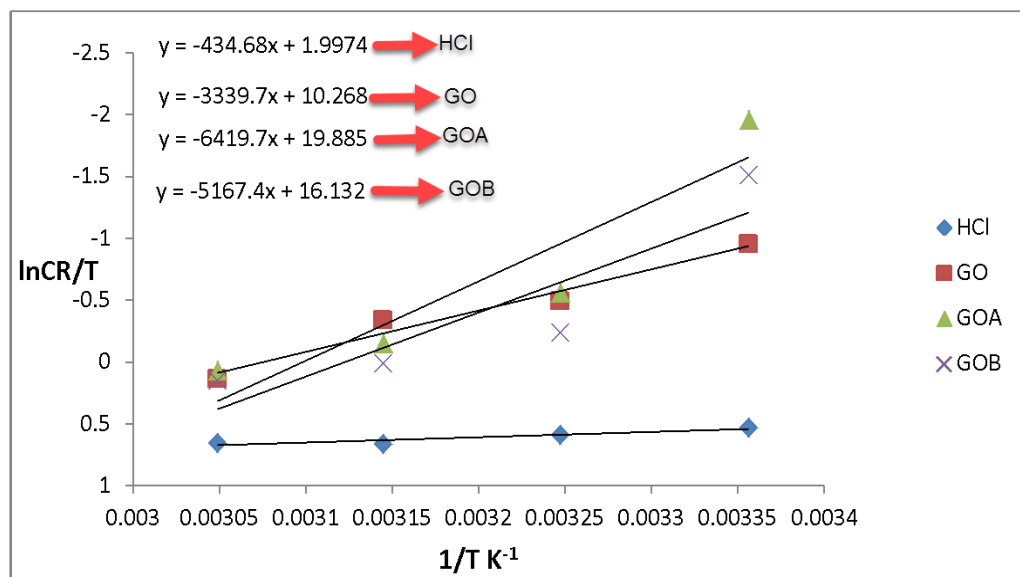


Figure 12: Calculation of  $\Delta H^*$  and  $\Delta S^*$  in the presence and absence of GO, GOA, and GOB.

In the present work, some isotherms, such as Timken, Langmuir, Frumkin, and Freundlich, are used. The best-fitted model among them for GO and its derivatives is Langmuir isotherm because it provides  $R^2$  that is close to one, as shown in Figure 13. The Langmuir isotherm is dependent on the assumption that all adsorption process sites are equivalent. This isotherm can be calculated using Equation 5:

$$\frac{C_{inhi}}{\theta} = \frac{1}{K} + C_{inhib} \dots\dots\dots 5$$

Where  $\theta$  is the surface coverage,  $C$  is the concentration of the inhibitor in parts per million, and  $K$  is the equilibrium constant of adsorption.  $K$  is determined from the Langmuir isotherm in Equation 5 for the

optimal concentration at different temperatures, as shown in Figure 13 [49, 50]. The Langmuir isotherms at optimal concentrations and different temperatures of organic compounds in 0.1 M HCl are plotted, as shown in Figure 13 and Table 10.

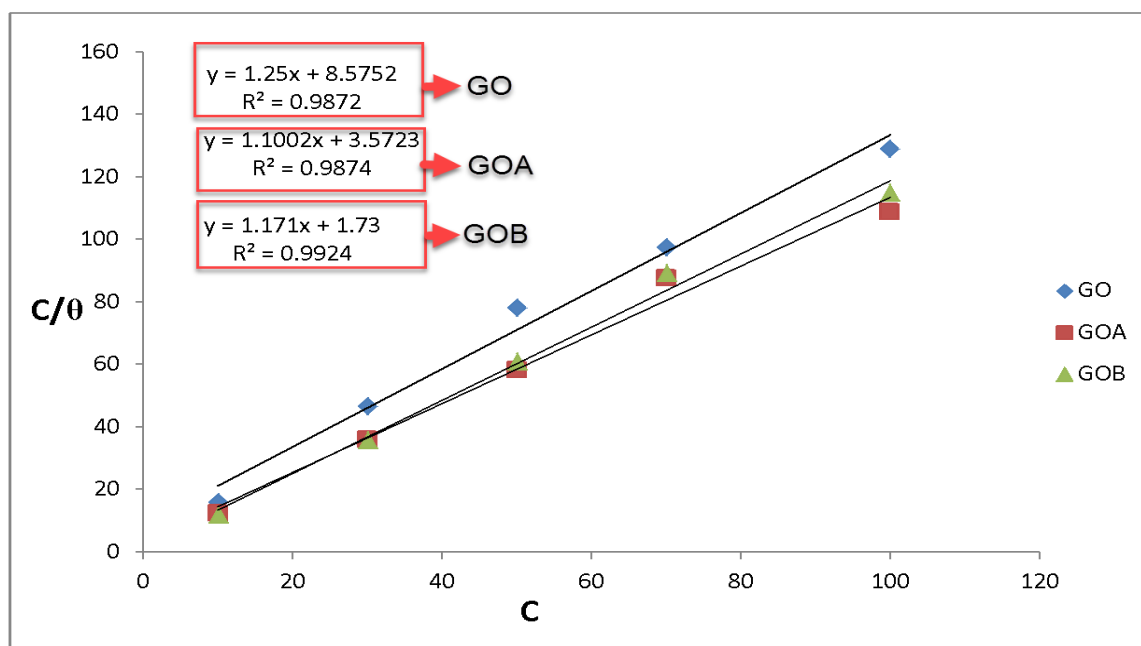


Figure 13: Langmuir adsorption isotherm plots of GO, GOA, and GOB.

Table 10: Langmuir adsorption isotherm of the synthesized compounds at 298 K.

Comp	Conc. (mg.L <sup>-1</sup> )	θ	C/θ	R <sup>2</sup>
GO	10	0.623	16.06	0.9872
	30	0.642	46.73	
	50	0.639	78.25	
	70	0.717	97.63	
	100	0.774	129.2	
GOA	10	0.792	12.63	0.9874
	30	0.828	36.24	
	50	0.858	58.28	
	70	0.798	87.72	
	100	0.917	109.05	
GOB	10	0.842	11.88	0.9924
	30	0.834	35.98	
	50	0.821	60.90	
	70	0.783	89.40	
	100	0.870	114.95	

#### 4. Conclusion

GO, GOA, and GOB were synthesized and evaluated as corrosion inhibitors of carbon steel alloy in 0.1 N HCl. The corrosion inhibition efficiency increased as the concentration increased at 25 °C at an optimal concentration of 100 ppm for GO, GOA, and GOB. All inhibitors were physically adsorbed on the surface of the carbon steel alloy to reduce corrosion that occurs in an acidic corrosive medium. This finding shows the effect of temperature on corrosion and the adsorption ability of the inhibitors on the

surface alloy. The inhibition efficiency of GOA was greater than that of other inhibitors, and this parameter showed the following order: GOA>GOB> GO. This order indicates that urea and thiourea were uniformly functionalized on the GO surface, and they enhanced the inhibition efficiency of GO. However, the degree of functionalization of urea was greater than that of thiourea. Therefore, the efficiency of GOA and GOB at 100 ppm was 91.7% and 84.2%, respectively. These inhibitors behaved as mixed inhibitors. The adsorption of the inhibitors follows Langmuir's adsorption isotherm because of  $R^2$ , which is close to unity.

## References

1. Deepak Dwivedi, Katerina Lepkova, and Thomas Becker, Carbon steel corrosion: a review of key surface properties and characterization methods. *RSC Advances*, 7 ( 2017) 4580-4610. [https://doi: 10.1039/c6ra25094g](https://doi.org/10.1039/c6ra25094g)
2. A S PATEL, V A PANCHAL and N K SHAH, Electrochemical impedance study on the corrosion of Al-Pure in hydrochloric acid solution using Schiff bases. *Bulletin of Materials Science*, 35 (2012) 283-290. <https://doi.org/10.1007/s12034-012-0270-1>
3. Ji Yang, Juan Peng, Zheming Shen, Jinping Jia, Feng Zhang, Corrosion protection of iron in water by activated carbon fiber (ACF). *Carbon*, 44 (2006) 19-26. <https://doi.org/10.1016/j.carbon.2005.07.006>
4. E. M. Fayyad, M. A. Almaadeed , A. Jones , A. M. Abdullah, Evaluation techniques for the corrosion resistance of self-healing coatings, *Int. J. Electrochem. Sci.*, 9 (2014) 4989 - 5011. <http://hdl.handle.net/10576/4594>
5. Mudigere Krishnegowda Pavithra, Thimmappa Venkatarangaiah Venkatesha, Mudigere Krishnegowda Punith Kumar, Nanjanagudu Subba Rao Anantha, , Outstanding inhibitive effect of colchicine on aluminium alloy 6061 corrosion. *Journal of Electrochemical Science and Engineering*, 5 (2015) 197-208. <https://doi.org/10.5599/jese.185>
6. Aprael S. Yaro , Anees A. Khadom, Rafal K. Wael, Apricot juice as green corrosion inhibitor of mild steel in phosphoric acid. *Alexandria Engineering Journal*, 52 (2013) 129-135. <https://doi.org/10.1016/j.aej.2012.11.001>
7. B. E. Amitha Rani and Bharathi Bai J. Basu, Green inhibitors for corrosion protection of metals and alloys: an overview. *International Journal of corrosion*, 380217 (2012) 1-3. <https://doi.org/10.1155/2012/380217>
8. Houyi Ma, Shenhao Chen, Bingsheng Yin , Shiyong Zhao , Xiangqian Liu, Impedance spectroscopic study of corrosion inhibition of copper by surfactants in the acidic solutions. *Corrosion Science*, 45 (2003) 867-882. [https://doi.org/10.1016/S0010-938X\(02\)00175-0](https://doi.org/10.1016/S0010-938X(02)00175-0)
9. Zongxue Yu, Liang Lv , Yu Ma , Haihui Di , Yi He, Covalent modification of graphene oxide by metronidazole for reinforced anti-corrosion properties of epoxy coatings. *RSC Advances*, 6 (2016) 18217-18226. <http://doi.org/10.1039/C5RA23595B>
10. Safina Iram Javed, Zakir Hussain, Covalently functionalized graphene oxide–characterization and its electrochemical performance. *Int. J. Electrochem. Sci*, 10 (2015) 9475-9487. <https://doi.org/10.0000/www.electrochemsci.org/vol10/101109475>
11. F Pendolino, N Armata, Graphene oxide in environmental remediation process. (2017) 1-51, Online ISBN 978-3-319-60429-9: <https://doi.org/10.1007/978-3-319-60429-9>
12. Paulchamy , Arthi and Lignesh, A simple approach to stepwise synthesis of graphene oxide nanomaterial. *J Nanomed Nanotechnol*,6 (2015) 1. [doi: 10.4172/2157-7439.1000253](https://doi.org/10.4172/2157-7439.1000253)
13. Alireza Ashori , Hossein Rahmani, Reza Bahrami, Preparation and characterization of functionalized graphene oxide/carbon fiber/epoxy nanocomposites. *Polymer Testing*, 48(2015)82-88. <https://doi.org/10.1016/j.polymertesting.2015.09.010>
14. J-L. Yan, G.J.Chen, J. Cao, W. Yang, B-H. Xie, M-B. Yang, Functionalized graphene oxide with ethylenediamine and 1, 6-hexanediamine. *New Carbon Materials*, 27 (2012) 370-376. [https://doi.org/10.1016/S1872-5805\(12\)60022-5](https://doi.org/10.1016/S1872-5805(12)60022-5)
15. Zongxue Yu, Yu Ma, Yi He, Ling Liang , Liang Lv , Xiang Ran , Yang Pan , Zhi Luo , Preparation of graphene oxide modified by titanium dioxide to enhance the anti-corrosion performance of epoxy coatings. *Surface and Coatings Technology*, 276 (2015) 471-478. <http://doi.org/10.1016/j.surfcoat.2015.06.02>
16. Sumita Rani, Dinesh Kumar, Mukesh Kumar, Improvement in humidity sensing of graphene oxide by amide functionalization. *Sensors & Transducers*, 193 (2015) 100. [https://www.sensorsportal.com/HTML/DIGEST/october\\_2015/Vol\\_193/P\\_2742](https://www.sensorsportal.com/HTML/DIGEST/october_2015/Vol_193/P_2742).

17. LEILA SHAHRIARY, ANJALI A. ATHAWALE, Graphene oxide synthesized by using modified hummers approach. *Int. J. Renew. Energy Environ. Eng.*, 2 (2014) 58-63.
18. Chi-Wei Lo, Difeng Zhu and Hongrui Jiang, An infrared-light responsive graphene-oxide incorporated poly (N-isopropylacrylamide) hydrogel nanocomposite. *Soft Matter*, 7 (2011) 5604-5609. [http:// doi: 10.1039/c1sm00011j](http://doi:10.1039/c1sm00011j)
19. Chenzhen Zhang, Rui Hao, Hanbin Liao, Yanglong Hou, Synthesis of amino-functionalized graphene as metal-free catalyst and exploration of the roles of various nitrogen states in oxygen reduction reaction. *Nano Energy*, 2(2013) 88-97. <https://doi.org/10.1016/j.nanoen.2012.07.021>
20. C. C. Caliman, A. F. Mesquita, D. F. Cipriano, J. C. C. Freitas, A. A. C. Cotta, W. A. A. Macedo and A. O. Porto, One-pot synthesis of amine-functionalized graphene oxide by microwave-assisted reactions: an outstanding alternative for supporting materials in supercapacitors. *RSC advances*, 8 (2018) 6136-6145. [http:// doi: 10.1039/C7RA13514A](http://doi:10.1039/C7RA13514A)
21. Zhen-Huan Sheng, Lin Shao, Jing-Jing Chen, Wen-Jing Bao, Feng-Bin Wang, and Xing-Hua Xia, Catalyst-free synthesis of nitrogen-doped graphene via thermal annealing graphite oxide with melamine and its excellent electrocatalysis. *ACS nano*, 2011. 5(6): p. 4350-4358. <https://doi.org/10.1021/nn103584t>
22. Grzegorz Sobon, Jaroslaw Sotor, Joanna Jagiello, Rafal Kozinski, Mariusz Zdrojek, Marcin Holdynski, Piotr Paletko, Jakub Boguslawski, Ludwika Lipinska, and Krzysztof M. Abramski Graphene oxide vs. reduced graphene oxide as saturable absorbers for Er-doped passively mode-locked fiber laser. *Optics express*, 20(2012) 19463-19473. <https://doi.org/10.1364/OE.20.019463>
23. Abhisek Gupta, Bikash Kumar Shaw and Shyamal Kumar Saha, Photoluminescence study of optically active diaminopyridine intercalated graphene oxide. *RSC Advances*, 4 (2014) 50542-50548. [http:// doi: 10.1039/c0xx00000x](http://doi:10.1039/c0xx00000x)
24. Kamila Żelechowska, Marta Przeźniak-Welenc, Marcin Łapiński, Izabela Kondratowicz and Tadeusz Miruszewski, Fully scalable one-pot method for the production of phosphonic graphene derivatives. *Beilstein journal of nanotechnology*, 8 (2017) 1094-1103. [http:// doi:10.3762/bjnano.8.111](http://doi:10.3762/bjnano.8.111)
25. Zhigang Mou, Xiaoye Chen, Yukou Du, Xiaomei Wang, Ping Yang, Suidong Wang, Forming mechanism of nitrogen doped graphene prepared by thermal solid-state reaction of graphite oxide and urea. *Applied Surface Science*, 258 (2011)1704-1710. <https://doi.org/10.1016/j.apsusc.2011.10.019>
26. Bing Xue, Jiagui Zhu, Na Liu, Yongxin Li, Facile functionalization of graphene oxide with ethylenediamine as a solid base catalyst for Knoevenagel condensation reaction. *Catalysis Communications*, 64 (2015) 105-109. <https://doi.org/10.1016/j.catcom.2015.02.003>
27. Akhil V. Nakhate and Ganapati D. Yadav, Synthesis and characterization of sulfonated carbon-based graphene oxide monolith by solvothermal carbonization for esterification and unsymmetrical ether formation. *ACS Sustainable Chemistry & Engineering*, 4 (2016) 1963-1973. <https://doi.org/10.1021/acssuschemeng.5b01205>
28. Shweta Kumari, Amiya Shekhar, and Devendra. Pathak, Synthesis and characterization of a Cu (II) Schiff base complex immobilized on graphene oxide and its catalytic application in the green synthesis of propargylamines. *RSC Advances*, 6 (2016)15340-15344. [http:// doi: 10.1039/x0xx00000x](http://doi:10.1039/x0xx00000x)
29. Nadeem Baig, D. S. Chauhan Tawfik A. Saleh and M. A. Quraishi, Diethylenetriamine functionalized graphene oxide as a novel corrosion inhibitor for mild steel in hydrochloric acid solutions. *New Journal of Chemistry*, 43 (2019) 2328-2337. [http:// doi: 10.1039/C8NJ04771E](http://doi:10.1039/C8NJ04771E)
30. Mohd Hazani Mat Zaid and Jaafar Abdullah, Preparation and characterization of amine functionalized graphene oxide with water soluble quantum dots for sensing material. in AIP Conference Proceedings. 1877 (2017)040002.. <https://doi.org/10.1063/1.4999868>
31. Himanshu Kharkwal , H.C. Joshi, K.P. Singh, Fabrication and Characterization of Layered Graphene Oxide Biocompatible Nano-Film by Various Methods. *International Journal of Biochemistry and Biophysics* 6 (2018) 1-19 . <https://doi.org/10.13189/ijbb.2018.060101>
32. Pankaj Gupta and Rajendra N. Goyal, Amino functionalized graphene oxide and polymer nanocomposite based electrochemical platform for sensitive assay of anti-doping drug atenolol in biological fluids. *Journal of the Electrochemical Society*, 163 (2016) B601-B608. [http://doi: 10.1149/2.0281613jes](http://doi:10.1149/2.0281613jes)
33. Aso Navae and Abdollah Salimi, Efficient amine functionalization of graphene oxide through the Bucherer reaction: an extraordinary metal-free electrocatalyst for the oxygen reduction reaction. *RSC Advances*, 5 (2015)59874-59880. [http:// doi: 10.1039/C5RA07892J](http://doi:10.1039/C5RA07892J)
34. D. Bouša J. Luxa , V. Mazánek , O. Jankovský , D. Sedmidubský , K. Klímová , M. Pumera and Z. Sofer, Toward graphene chloride: chlorination of graphene and graphene oxide. *RSC Advances*, 6 (2016)66884-66892. [https:// doi: 10.1039/C6RA14845J](https://doi:10.1039/C6RA14845J)

35. Yuan-Hsiang Yu, Yan-Yu Lin, Chia-Hsuan Lin, Chih-Chieh Chan and Ying-Chieh Huang, High-performance polystyrene/graphene-based nanocomposites with excellent anti-corrosion properties. *Polymer Chemistry*, 5 (2014)535-550. [http:// doi: 10.1039/C3PY00825H](http://doi:10.1039/C3PY00825H)
36. WON-CHUN OH, and FENG-JUN ZHANG, Preparation and characterization of graphene oxide reduced from a mild chemical method. *Asian Journal of Chemistry*, 23(2) (2011) 875- 878.
37. LinfeiLai, LuweiChen, DaZhan, LiSun, JinpingLiu, San HuaLim, Chee KokPoh, ZexiangShen, JianyiLin, One-step synthesis of NH<sub>2</sub>-graphene from in situ graphene-oxide reduction and its improved electrochemical properties. *Carbon*, 49 (2011) 3250-3257. <https://doi.org/10.1016/j.carbon.2011.03.051>
38. Ahmad Monshi , Mohammad Reza Foroughi, Mohammad Reza Monshi, Modified Scherrer equation to estimate more accurately nano-crystallite size using XRD. *World journal of nano science and engineering*, 2 (2012) 154-160. [http:// doi:10.4236/wjnse.2012.23020](http://doi:10.4236/wjnse.2012.23020)
39. A. Ostovari, S.M. Hoseinieh , M. Peikari , S.R. Shadizadeh , S.J. Hashemi, Corrosion inhibition of mild steel in 1 M HCl solution by henna extract: A comparative study of the inhibition by henna and its constituents (Lawsonic acid, Gallic acid,  $\alpha$ -D-Glucose and Tannic acid). *Corrosion Science*, 51 (2009) 1935-1949. [http:// doi:10.1016/j.corsci.2009.05.024](http://doi:10.1016/j.corsci.2009.05.024)
40. R.T. Loto, and C.A. Loto, Effect of p-phenylenediamine on the corrosion of austenitic stainless steel type 304 in hydrochloric acid. Effect of P-Phenylenediamine on the Corrosion of Austenitic Stainless Steel Type 304 in Hydrochloric Acid, *Int. J. Electrochem. Sci*, 7 (2012) 9423 - 9440. <http://eprints.covenantuniversity.edu.ng/id/eprint/1468>
41. H. Serrar , M. Larouj, H.L. Gaz, Z. Benzekri , A. Zarguil , H. Essebaai , S. Boukhris , H. Oudda , R. Salghi , A. Hassikou and A. Souizi, Experimental and Theoretical Studies of the Corrosion Inhibition of 4-amino-2-(4-chlorophenyl)-8-(2, 3-dimethoxyphenyl)-6-oxo-2, 6-dihydropyrimido [2, 1-b][1, 3] thiazine-3, 7-dicarbonitrile on Carbon Steel in a 1.0 M HCl Solution. *Portugaliae Electrochimica Acta*, 36 (2018)35-52. <http://dx.doi.org/10.4152/pea.201801035>
42. Al-Sawaad, H.Z., Ph.D. Thesis. College of science, University of Basrah, 2010.
43. Hadi Z. Al-Sawaad, Naem T. Faili and Ali. H. Essa, Evaluation of Vicine as a Corrosion Inhibitor for Carbon Steel Alloy. *Portugaliae Electrochimica Acta*, 37 (2019) 205-216. [http:// doi: 10.4152/pea.201904205](http://doi:10.4152/pea.201904205)
44. P.C. Okafor, V.I. Osabor and E.E. Ebenso, Eco-friendly corrosion inhibitors: inhibitive action of ethanol extracts of *Garcinia kola* for the corrosion of mild steel in H<sub>2</sub>SO<sub>4</sub> solutions. *Pigment & Resin Technology*, 36 (2007) 299-305. [http:// doi/10.1108/03699420710820414/full/html](http://doi/10.1108/03699420710820414/full/html)
45. Hadi Z.M. Al-Sawaad, Alaa S.K. Al-Mubarak, Athir M. Haddad, The inhibition effects of dimethylol-5-methyl hydantoin and its derivatives on carbon steel alloy. *J. Mater. Environ. Sci*, 1 (2010) 227-238.
46. J Ishwara Bhat and Vijaya Alva, Corrosion inhibition of aluminium by 2-chloronicotinic acid in HCl medium. *Indian Journal of Chemical Technology* 16(2009) 228-233.
47. M.J. Bahrami , S.M.A. Hosseini, P. Pilvar, Experimental and theoretical investigation of organic compounds as inhibitors for mild steel corrosion in sulfuric acid medium. *Corrosion science*, 52 (2010) 2793-2803. <https://doi.org/10.1016/j.corsci.2010.04.024>
48. Abdulkareem Mohammed Ali Al-Sammarraie and Mazin Hasan Raheema, Electrodeposited reduced graphene oxide films on stainless steel, copper, and aluminum for corrosion protection enhancement. *International Journal of Corrosion*, 6939354 (2017) 1-8. <https://doi.org/10.1155/2017/6939354>
49. M. Lebrini, F. Robert, and C. Roos, Adsorption properties and inhibition of C38 steel corrosion in hydrochloric solution by some indole derivatives: temperature effect, activation energies, and thermodynamics of adsorption. *International Journal of corrosion*, 139798(2013) 1-13. <http://dx.doi.org/10.1155/2013/139798>
50. Layla A. Al Juhaiman, Polyvinyl pyrrolidone as a corrosion inhibitor for carbon steel in HCl. *International Journal of Electrochemical Science*, 11 (2016) 2247-2262.
51. M. Lebrini, F. Robert, , P.A. Blandinières, C. Roos, Corrosion inhibition by *Isertia coccinea* plant extract in hydrochloric acid solution. *Int. J. Electrochem. Sci*, 6 (2011) 2443-2460. <http://citeseerx.ist.psu.edu/viewdoc/download?doi=10.1.1.655.5791&rep=rep1&type=pdf>
52. M. Dahmani, A. Et-Touhami , S.S. Al-Deyab , B. Hammouti, A. Bouyanzer , Corrosion inhibition of C38 steel in 1 M HCl: A comparative study of black pepper extract and its isolated piperine. *Int. J. Electrochem. Sci*, 5 (2010) 1060-1069. <http://www.electrochemsci.org/papers/vol5/5081060.pdf>

(2020) ; <http://www.jmaterenvironsci.com>